Magnetic Reconnection in the Interior of Interplanetary Coronal Mass Ejections

R. L. Fermo and M. Opher
Center for Space Physics, Astronomy Department, Boston University, Boston, Massachusetts 02215, USA

J. F. Drake
Institute for Research in Electronics and Applied Physics, Department of Physics, University of Maryland, College Park, Maryland 20742-3511, USA

(Received 30 June 2013; published 16 July 2014)

Recent *in situ* observations of interplanetary coronal mass ejections (ICMEs) found signatures of reconnection exhausts in their interior or trailing edge. Whereas reconnection on the leading edge of an ICME would indicate an interaction with the coronal or interplanetary environment, this result suggests that the internal magnetic field reconnects with itself. In light of this data, we consider the stability properties of flux ropes first developed in the context of astrophysics, then further elaborated upon in the context of reversed field pinches (RFPs). It was shown that the lowest energy state of a flux rope corresponds to $\nabla \times \mathbf{B} = \lambda \mathbf{B}$ with λ a constant, the so-called Taylor state. Variations from this state will result in the magnetic field trying to reorient itself into the Taylor state solution, subject to the constraints that the toroidal flux and magnetic helicity are invariant. In reversed field pinches, this relaxation is mediated by the reconnection of the magnetic field, resulting in a sawtooth crash. If we likewise treat the ICME as a flux rope, any deviation from the Taylor state will result in reconnection within the interior of the flux tube, in agreement with the observations by Gosling *et al*. Such a departure from the Taylor state takes place as the flux tube cross section expands in the latitudinal direction, as seen in magnetohydrodynamic (MHD) simulations of flux tubes propagating through the interplanetary medium. We show analytically that this elongation results in a state which is no longer in the minimum energy Taylor state. We then present magnetohydrodynamic simulations of an elongated flux tube which has evolved away from the Taylor state and show that reconnection at many surfaces produces a complex stochastic magnetic field as the system evolves back to a minimum energy state configuration.

DOI: 10.1103/PhysRevLett.113.031101 PACS numbers: 96.60.ph, 96.50.Bh, 96.50.Uv, 96.60.Iv

Coronal mass ejections (CMEs) are bursts of plasma released from the solar corona into space, carrying as much as 10^{16} grams of mass and 10^{30} ergs of energy out into the interplanetary medium [1–3]. The ejecta usually are carried out into the interplanetary medium [as an interplanetary coronal mass ejection (ICME)] by closed magnetic fields, typically described as having a flux rope geometry. When this is observed as a smooth rotation in the magnetic field, the ICME is classified as a magnetic cloud [4,5]. A coherent helical flux rope geometry is not always observed, however, as magnetic clouds comprise perhaps only 30% of observed ICMEs [6]. When directed towards Earth, CMEs can generate geomagnetic storms in the magnetosphere [7,8]. The most energetic solar energetic particles (SEPs) may approach 80% of the speed of light, yet the mechanism which produces SEPs remains an open question. Diffusive shock acceleration, whereby particles gain energy by first order Fermi acceleration at the shock which forms at the fore of a fast CME, has been suggested as one such mechanism [9,10]. Alternatively, impulsive SEP events observed in the interplanetary medium have been correlated with flare acceleration in the lower corona [9], perhaps suggestive of magnetic reconnection as a SEP acceleration mechanism.

Consequently, magnetic reconnection plays a very important role in CME dynamics, whether in the acceleration of SEPs, in triggering the flare event, or in driving flux rope expansion. If the ICME flux rope were analogous to Earth's magnetosphere, one might expect to find these reconnection events either at the leading edge where the ICME magnetic field most directly interacts with the interplanetary magnetic field (as in the magnetopause) or in the trailing edge behind the flux rope where the magnetic field pinches off (as in the magnetotail). Surprisingly though, many of the reconnection exhausts observed by the Ulysses spacecraft were found within the interiors of ICMEs [11], regions characterized by counterstreaming electrons and very low proton beta $\beta = 8\pi nT/B^2$.

In light of this result, we consider the disruptive role that magnetic reconnection plays in fusion plasmas. It was in this context that the linear tearing mode instability that initiates reconnection was developed [12]. In 1974, Taylor published a seminal Letter which linked reconnection events in reversed field pinches (RFPs) with relaxation towards the minimum energy state (since dubbed the Taylor state) which satisfies the force-free condition

$$\nabla \times \mathbf{B} = \lambda \mathbf{B}, \tag{1}$$

with λ a constant [13]. That a force-free magnetic field corresponds to the lowest energy state had already been established in the context of astrophysical plasmas [14]. However, Taylor went further by suggesting that, for an RFP geometry subject to the constraints that the toroidal magnetic flux $\Phi = \int_A \mathbf{B} \cdot d\mathbf{n}$ through a cross-sectional area A and the magnetic helicity $K = \int_V \mathbf{A} \cdot \mathbf{B} d\tau$ (where $\mathbf{A}$ is the magnetic potential) are invariant, then the relaxation of the plasma back towards the Taylor state must be carried out by reconnection [13,15]. This manifests itself in RFP discharges as a sawtooth crash [16]. If the profile of the safety factor $q = 2\pi r B_z / L_z B_\theta$ as a function of poloidal radius r is equal to a rational value $q = m/n$ at some r where m and n are integers, then one may transform into a frame which rotates with the local magnetic field. In that twisted frame, the magnetic field reverses across r and can reconnect across that surface.

If we likewise treat the ICME as a flux rope, any variation from the Taylor state will result in reconnection within the interior of the ICME, in accord with the observations of Gosling *et al.* [11,17]. The flux rope may begin in a force-free Taylor state which satisfies Eq. (1) when it first forms, as there is enough time for the system to relax into its minimum energy state [18,19]. However, the ICME may not remain in such a state once it erupts and begins to propogate outwards into the interplanetary medium, where the ICME and its environs become highly dynamic systems. This departure from the minimum energy Taylor state occurs in ICMEs through the elongation of the flux tube in the latitudinal direction. As the flux tube propagates through the interplanetary medium, at distances far from the sun the azimuthal magnetic field falls as $1/r$, and so the magnetic flux must expand. The radial velocity does not vary significantly over the course of the propagation of the ICME, so the expansion must occur in the latitudinal direction [20]. In 3D global MHD simulations of a Gibson-Low flux rope model [21] for a CME, as the flux rope propagates through the interplanetary medium, the ICME cross section becomes elongated into an ellipse, with its major axis in the latitudinal direction [22]. ICME flux ropes modeled with this elongation yield better fits with observational data than those which employ cylindrical symmetry [23–25].

We now show that such an elongation of the flux rope cross section results in deviation from the Taylor state, which will require reconnection in order to relax back towards the minimum energy solution Eq. (1). Here, we shall consider the solution in a Cartesian geometry, for which we can easily apply the transformation $x \to x/2$, $y \to 2y$ to mimic the elongation of the flux rope in the latitudinal direction x. We consider a domain of size $L_x \times L_y \times L_z$ with conducting boundaries in x and y and periodic in z. The Taylor state solution has the form

$$B_x = -B_0 \sqrt{\frac{L_x}{L_y}} \cos\left(\frac{\pi x}{L_x}\right) \sin\left(\frac{\pi y}{L_y}\right), \tag{2}$$

$$B_y = B_0 \sqrt{\frac{L_y}{L_x}} \sin\left(\frac{\pi x}{L_x}\right) \cos\left(\frac{\pi y}{L_y}\right), \tag{3}$$

$$B_z = B_{z0} \cos\left(\frac{\pi x}{L_x}\right) \cos\left(\frac{\pi y}{L_y}\right). \tag{4}$$

This solves Eq. (1) with $\lambda = \pi \sqrt{1/L_x^2 + 1/L_y^2}$ and

$$B_{z0} = B_0 \sqrt{\frac{L_x^2 + L_y^2}{L_x L_y}}. \tag{5}$$

Figure 1 illustrates the Taylor state solutions described by Eqs. (2)–(4) for (a) $L_x = L_y = L = 4$, and (b) $L_x = 8$, $L_y = 2$, $L_z = 4$. The contour lines trace the poloidal magnetic fields B_x and B_y in that plane. The flux function ψ defined such that $\mathbf{B} = \hat{z} \times \nabla\psi + B_z \hat{z}$ is given by $\psi = B_z/\lambda$ so that the magnetic field lines shown in Fig. 1 are also contours of B_z in the x-y plane. Near the origin, a Taylor expansion about $x = y = 0$ yields

$$\psi \approx \frac{B_0}{\pi} \sqrt{L_x L_y} \left(1 - \frac{\pi^2}{2L^2} r^2\right), \tag{6}$$

under the transformation $r^2 = \alpha^{-2} x^2 + \alpha^2 y^2$, where $L = \sqrt{L_x L_y}$ and $\alpha = \sqrt{L_x/L_y} = L_x/L = L/L_y$. The center of our Cartesian flux tube approaches the more realistic case of an elliptical flux tube near its center.

For this solution, one can calculate the two invariants detailed in Taylor [15]:

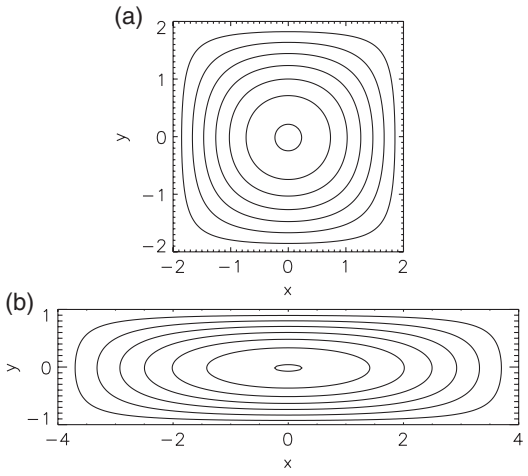

FIG. 1. The in-plane magnetic field of the Taylor state solution in Eqs. (2)–(3). The field lines also act as contour levels of B_z as defined in Eq. (4).

$$\Phi = \int_A B_z dA = \frac{4}{\pi^2} B_0 \sqrt{L_x L_y (L_x^2 + L_y^2)}, \quad (7)$$

$$K = \int d\tau \mathbf{A} \cdot \mathbf{B} = \frac{B_0^2}{2\pi} L_x L_y L_z \sqrt{L_x^2 + L_y^2}. \quad (8)$$

Consider now a flux tube which initially satisfies $L_x = L_y = L$, with toroidal flux $\Phi_0 = 4\sqrt{2} B_0 L^2/\pi^2$ and magnetic helicity $K_0 = B_0^2 L^3 L_z/\sqrt{2}\pi$. Suppose some dynamic process compresses the flux tube in y while maintaining the total cross sectional area L^2, say to $L_x = \alpha L$, $L_y = L/\alpha$. With this aspect ratio, the minimum energy Taylor state described by Eqs. (2)–(4) would now have toroidal flux $\Phi_1 = \sqrt{\alpha^2/2 + 1/2\alpha^2}\Phi_0$ and magnetic helicity $K_1 = \sqrt{\alpha^2/2 + 1/2\alpha^2} K_0$. Since these quantities are to remain invariant, the resultant flux tube, elongated in one cross-sectional direction, will have deviated from the Taylor state, and, consequently, reconnection will commence.

To test this, we perform magnetohydrodynamic (MHD) simulations of a magnetic flux rope using the F3D code [26]. We utilize periodic boundaries in x and z but conducting boundaries along the longer (when simulating the elongated flux rope) y boundary. Thus, the simulation domain is $-L_x < x < L_x$, $-L_y/2 < y < L_y/2$, and $-L_z/2 < z < L_z/2$, which actually describes two flux ropes horizontally adjacent to one another. Equations (2)–(4) are still valid as the solution for this system, but we shall focus solely on the flux rope in the region $-L_x/2 < x < L_x/2$, $-L_y/2 < y < L_y/2$. The system is initialized with Eqs. (2)–(4) with $B_0 = 0.5$, constant temperature $T_i = T_e$, background density $n_0 = 1$, and no explicit resistivity, although there is a fourth-order dissipation term of the form $\mu_4 \nabla^4$. The system is normalized to an arbitrary length scale L, velocities to the Alfvén speed v_A, and time to L/v_A.

In our first simulation, we begin with the cylindrical case: $L_x = L_y = 8$, $L_z = 4$. Using the Taylor state equilibrium defined by Eqs. (2)–(4), the solution remains in a near steady-state equilibrium. Substituting for B_0, L_x, and L_y into Eq. (5), the amplitude of B_z is $B_{z0} = 1/\sqrt{2}$.

In simulating the elliptical case, with $L_x = 16$, $L_y = 4$, $L_z = 4$, we again start with a magnetic field configuration of the form described by Eqs. (2)–(4). However, we wish to simulate a system which might have evolved from the cylindrical case. In order to maintain the invariance of the toroidal flux Φ and magnetic helicity K of the cylindrical case, the amplitude of the elliptical flux rope must also have amplitude $B_{z0} = 1/\sqrt{2}$. Note, however, that this amplitude differs from the amplitude of B_z which would satisfy the force-free condition Eq. (1) for the Taylor state solution, namely, $B_{z0} = \sqrt{17}/4$ as determined by Eq. (5) for the parameters of the elliptical case.

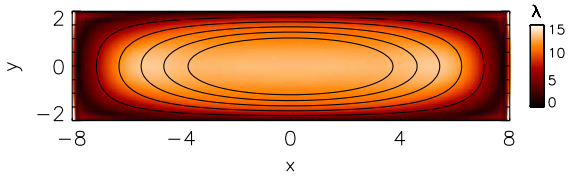

FIG. 2 (color online). The equilibrium state for the $L_x = 16$, $L_y = 4$ case which satisfies Eq. (1) but only for nonconstant λ. The color bar shows $\lambda = 4\pi \mathbf{J} \cdot \mathbf{B}/B^2$, while contour lines depict the in-plane magnetic field $B_x - B_y$, as contours of the flux function ψ.

Using instead $B_{z0} = 1/\sqrt{2}$ initializes the flux rope with the same toroidal flux and magnetic helicity as the cylindrical case, but in a state which is out of magnetohydrodynamic equilibrium because it does not satisfy Eq. (1). We therefore start with a 2D MHD simulation with Eqs. (2)–(4), using $B_{z0} = 1/\sqrt{2}$ in place of that calculated in Eq. (5). We evolve the system in time and zero out the flows regularly until it settles into an approximate equilibrium state. The final state satisfies Eq. (1), but with a nonconstant λ as shown in Fig. 2. As a result, when we extend this configuration into a 3D system, even with no initial variation in z save for an initial perturbation, we find that this equilibrium is unstable. Figure 3 shows the magnetic energy in the simulation domain as a function of time, which shows that around 5% of the magnetic energy is dissipated by reconnection by $t = 1000$.

Figure 3 suggests that reconnection is strongest over the period from $t = 200$ to $t = 400$. We now seek to find out where reconnection is occurring. For this purpose, we use puncture plots in which one traces a magnetic field line and places a point in the x-y plane each time that field line crosses a particular toroidal cross section (say, $z = 0$). Figure 4(a) shows the puncture plot of the initial configuration, Fig. 4(b) at $t = 150$, and Fig. 4(c) at $t = 200$.

We see that five distinct islands formed in the vicinity of the flux surface with x intercept $x_0 = 3$ [colored blue in Figs. 4(a)–4(c)]. This result matches well the expectation from the profile of the safety factor q in the initial configuration in Fig. 5, which shows that the flux surface with $q = 5$ has x intercept $x_0 \approx 2.8$. Further out in Fig. 4(a) at $x_0 \approx 6.0$, we also find five islands (in orange). Comparing with Fig. 5, we see that these islands correspond to the $q = 5/2$ rational surface. The orange flux

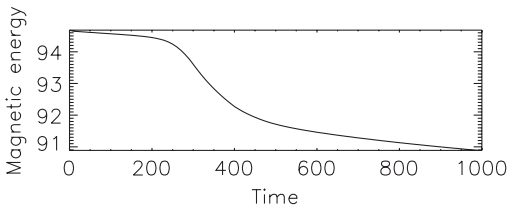

FIG. 3. The total magnetic energy in the simulation of the $L_x = 16$, $L_y = 4$ flux tube as a function of time.

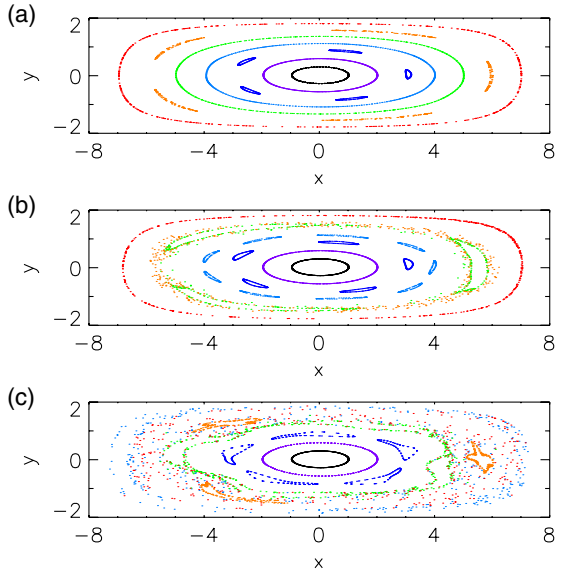

FIG. 4 (color online). Puncture plots at (a) $t = 50$ and (b) $t = 200$. Note that (b) is a zoom into $-4 < x < 4$, $-1 < y < 1$ to emphasize the structure in that region, and each color corresponds to the punctures of a unique flux surface. Each flux surface is traced starting from its x intercept at $x = 1, 2, \ldots, 7$; i.e., the black puncture points correspond to a flux surface traced from $x = 1$, $y = 0$, the violet at $x = 2$, $y = 0$, etc.

surface in Fig. 4(b) has broken up due to its interaction with the $q = 3$ island. The flux surface near $x_0 = 5$ has developed three magnetic islands (in green), corresponding to the $q = 3$ rational surface at $x_0 \approx 5.5$ in Fig. 5. Likewise, we find that nine magnetic islands form near $x_0 \approx 4.0$, corresponding to the $q = 9/2$ rational surface in Fig. 5. However, by the time we arrive at Fig. 4(c), we find that most of these islands have broken up, although remnants of the $q = 5$ and $q = 3$ islands are recognizable.

The change in magnetic topology coupled with the loss of magnetic energy in Fig. 3 indicate that reconnection has taken place at each of these rational surfaces. Figure 4 foreshadows the eventual fate of this flux tube: a stochastic magnetic field with a scattered puncture plot that has lost much of its original helical structure.

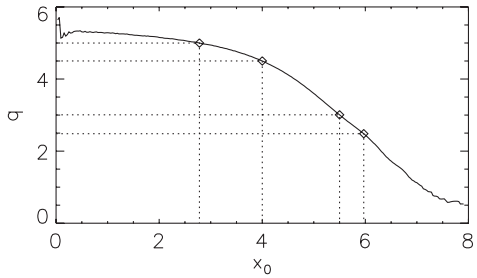

FIG. 5. The safety factor profile as a function of the x intercept x_0 of a given flux surface. The diamond markers denote rational flux surfaces highlighted in Fig. 4: those with $q = 5$ at $x_0 \approx 2.8$, $q = 9/2$ at $x_0 \approx 4.0$, $q = 3$ at $x_0 \approx 5.5$, and $q = 5/2$ at $x_0 \approx 6.0$.

Although these simulations are an idealization of a true ICME flux rope, the removal of these idealizations only reinforces the stochastic nature of the magnetic field. For instance, the interplanetary plasma is essentially collisionless so that a kinetic treatment will ultimately be needed. In the case of reconnection with a guide field the development of secondary magnetic islands [27,28] leads to a highly turbulent system [29]. This dynamic is further reinforced by fully 3D reconnection simulations in which secondary instabilities generate three-dimensional flux ropes [30]. Even just within a fluid context, the very high Lundquist numbers ($S > 10^{14}$) in the solar wind reside in the plasmoid-unstable regime [31–33]. Our simulations are already nonlaminar, even in a low Lundquist number fluid simulation, so the removal of these idealizations would only further underscore our results. One might also consider that the ICME flux rope will not be periodic in z but have footpoints anchored at the solar surface. Nevertheless, if the ICME propagation speed exceeds the local fast mode speed, then the interior of the flux tube cannot know about the footpoint boundaries. The flux tube length is essentially infinite, at which limit the separation between rational surfaces goes to zero. Our flux tube is long enough to simulate this effect since the rational surfaces are sufficiently close together to overlap in Fig. 4(c).

The results of this study are important for understanding the dynamics of interplanetary coronal mass ejections. They explain the observational data that reconnection is observed most frequently in the interior of the flux tubes by Gosling *et al.* [11,17]. If reconnection begins early enough in the life of the CME, then by 1 AU we might find that the structure lacks the helical flux rope configuration characteristic of magnetic clouds. This has been seen in many of the ICMEs observed at 1 AU, some of which observationally seem to show a helical flux rope structure, but as many as 70% of which do not [6]. In light of this Letter, current modeling techniques for mapping out the ICME flux rope structure as a helical flux rope may be overly simplistic.

The presence of reconnection sites within ICMEs could also be a source of SEP acceleration and lead to turbulence, both important topics for future research. The time scale for the degradation of the flux within the ICME will depend on such factors as the elongation aspect ratio (a measure of the variation from the Taylor state) and the reconnection rate. The former can be determined from observations, which suggest aspect ratios between 3 in 6, comparable to the aspect ratio of 4 in these simulations [24,25]. The latter will ultimately require a kinetic treatment, as collisionless physics would make reconnection fast enough to allow these processes to occur in the ICME between its ejection and 1 AU.

This work was supported by SHINE Grant No. AGS 1151422. Computations were performed at the National Energy Research Scientific Computing Center.

[1] J. T. Gosling, E. Hildner, R. M. MacQueen, R. H. Munro, A. I. Poland, and C. L. Ross, J. Geophys. Res. **79**, 4581 (1974).
[2] A. J. Hundhausen, in *Solar Wind Six*, Vol. 2, edited by V. Pizzo, T. E. Holzer, and D. G. Sime (NCAR, Estes Park, CO, 1987), p. 181.
[3] O. C. S. Syr, S. P. Plunkett, D. J. Michels, S. E. Paswaters, M. J. Koomen, G. M. Simnett, B. J. T. J. B. Gurman, R. Schwenn, D. F. Webb, E. Hildner, and P. L. Lamy, J. Geophys. Res. **105**, 18169 (2000).
[4] L. F. Burlaga, E. Sittler, F. Mariani, and R. Schwenn, J. Geophys. Res. **86**, 6673 (1981).
[5] L. W. Klein and L. F. Burlaga, J. Geophys. Res. **87**, 613 (1982).
[6] J. T. Gosling, in *Physics of Magnetic Flux Ropes*, Geophys. Monogr. Ser., edited by C. Russell, E. R. Priest, and L. C. Lee (American Geophysical Union, Washington, DC, 1990) p. 343.
[7] L. F. Burlaga, K. W. Behannon, and L. Klein, J. Geophys. Res. **92**, 5725 (1987).
[8] J. T. Gosling, J. Geophys. Res. **98**, 18937 (1993).
[9] D. V. Reames, Rev. Geophys. **33**, 585 (1995).
[10] I. I. Roussev, I. V. Sokolov, T. G. Forbes, T. I. Gombosi, M. A. Lee, and J. I. Sakai, Astrophys. J. Lett. **605**, L73 (2004).
[11] J. T. Gosling, S. Erkisson, R. M. Skoug, D. J. McComas, and R. J. Forsyth, Astrophys. J. **644**, 613 (2006).
[12] H. P. Furth, J. Killeen, and M. N. Rosenbluth, Phys. Fluids **6**, 459 (1963).
[13] J. B. Taylor, Phys. Rev. Lett. **33**, 1139 (1974).
[14] L. Woltjer, Astrophys. J. **128**, 384 (1958).
[15] J. B. Taylor, Rev. Mod. Phys. **58**, 741 (1986).
[16] R. G. Watt and R. A. Nebel, Phys. Fluids **26**, 1168 (1983).
[17] J. T. Gosling, R. M. Skoug, D. J. McComas, and C. W. Smith, J. Geophys. Res. **110**, A01107 (2005).
[18] M. Zhang and B. C. Low, Annu. Rev. Astron. Astrophys. **43**, 103 (2005).
[19] B. C. Low, Astrophys. J. **768**, 7 (2013).
[20] W. Poomvises, J. Zhang, and O. Olmedo, Astrophys. J. Lett. **717**, L159 (2010).
[21] S. E. Gibson and B. C. Low, Astrophys. J. **493**, 460 (1998).
[22] W. B. Manchester, T. I. Gombosi, I. Roussev, D. L. De Zeeuw, I. V. Sokolov, K. G. Powell, G. Toth, and M. Opher, J. Geophys. Res. **109**, A01102 (2004).
[23] M. J. Owens, V. G. Merkin, and P. Riley, J. Geophys. Res. **111**, A03104 (2006).
[24] N. P. Savani, M. J. Owens, A. P. Rouillard, R. J. Forsyth, K. Kusano, D. Shiota, and R. Kataoka, Astrophys. J. **731**, 109 (2011).
[25] N. P. Savani, M. J. Owens, A. P. Rouillard, R. J. Forsyth, K. Kusano, D. Shiota, R. Kataoka, L. Jian, and V. Bothmer, Astrophys. J. **732**, 117 (2011).
[26] M. A. Shay, J. F. Drake, M. Swisdak, and B. N. Rogers, Phys. Plasmas **11**, 2199 (2004).
[27] J. F. Drake, M. Swisdak, K. M. Schoeffler, B. N. Rogers, and S. Kobayashi, Geophys. Res. Lett. **33**, L13105 (2006).
[28] R. L. Fermo, J. F. Drake, and M. Swisdak, Phys. Rev. Lett. **108**, 255005 (2012).
[29] E. Leonardis, S. C. Chapman, W. Daughton, V. Roytershteyn, and H. Karimabadi, Phys. Rev. Lett. **110**, 205002 (2013).
[30] W. Daughton, V. Roytershteyn, H. Karimabadi, L. Yin, B. J. Albright, B. Bergen, and K. J. Bowers, Nat. Phys. **7**, 539 (2011).
[31] N. F. Loureiro, A. A. Schekochihin, and S. Cowley, Phys. Plasmas **14**, 100703 (2007).
[32] A. Bhattacharjee, Y.-M. Huang, H. Yang, and B. Rogers, Phys. Plasmas **16**, 112102 (2009).
[33] N. F. Loureiro, R. Samtaney, A. A. Schekochihin, and D. A. Uzdensky, Phys. Plasmas **19**, 042303 (2012).